

Removal of Ba(II) and Sr(II) ions using modified chitosan beads with pendent amidoxime moieties by batch and fixed bed column methods

A.F. Shaaban^a, T.Y. Mohamed^a, D.A. Fadel^{b,*}, N.M. Bayomi^a

^aChemistry Department, Faculty of Science, Benha University, Benha, Egypt, Tel. +201091174238, email: afshaaban@hotmail.com (A.F. Shaaban), Tel. +201284605833, email: dr_talaat2003@yahoo.com (T.Y. Mohamed), Tel. +201013998278, email: Chemist_nadamohamed_2012@yahoo.com (N.M. Bayomi)

^bNuclear Research Center, Atomic Energy Authority, P.O. 13759 Inshas, Cairo, Egypt, Tel. +201066211706, email: dalia_shaaban@windowslive.com (D.A. Fadel)

Received 8 January 2017; Accepted 13 April 2017

ABSTRACT

A new Modified chitosan beads with pendent amidoxime moieties (CACR) was prepared by reaction of cross-linking chitosan beads (CLCB) with acrylonitrile and hydroxylamine hydrochloride, respectively. The resulted chelating resin was characterized using FTIR Spectroscopy, thermal gravimetric analysis (TGA), differential scanning calorimeter (DSC), BET surface area, and scanning electron microscope (SEM- EDX). Batch adsorption experiments of strontium and barium from aqueous solution onto CACR has been investigated as a function of pH, metal ion concentration, contact time, metal ion concentration and temperature. Adsorption experiments indicated that the adsorption capacity was dependent on operating variables. The saturated adsorption capacities at 25°C were 2.30 and 1.75 mmol/g resin for Ba(II) and Sr(II), respectively. Equilibrium isotherm data were analyzed using Langmuir, Freundlich, and Temkin isotherm models, the equilibrium adsorption results were obviously fitted with Freundlich model. The kinetics data were well fitted by pseudo-second order kinetic model. Thermodynamic parameters were calculated for the uptake of the metal ions under study and it was found to be a spontaneous and endothermic process. The adsorption performance of CACR toward Ba(II) and Sr(II) using fixed bed column method was investigated under different conditions. Thomas and Yoon–Nelson models were applied to the experimental data to analyze the column performance. Regeneration was effectively performed using nitric acid and the chelating resin could be used repetitively for five times with little decrease (2–9%) in adsorption of metal ions.

Keywords: Modified chitosan; Amidoxime; Adsorption; Kinetics; Thermodynamics; Barium; Strontium

1. Introduction

Barium and strontium ions were classified as the most toxic metals present in radioactive liquid wastes arising from different sources including: inadequate activities for the management and disposal of radioactive waste, getting rid of radioactive items to the environment, nuclear activities, testing of nuclear weapons, nuclear fuel cycle processes, etc. Both of these ions are bone seeking metals and

hence have carcinogenic effects [1–3]. Presence of barium in aquatic environment can be related to some industries like (mining for example), as barium spread and dissolve easily in water of lakes, rivers and streams. By this cycle, barium can pass and deposit not only at the bodies of fish but also at any aquatic organisms by their absorption to barium ions from water. The great problem is that barium compounds can spread over large distances. When fish and other aquatic organisms absorb the barium compounds, barium will be sediment inside their bodies [3]. As it forms insoluble compounds with other common elements of the environment, such as carbonate and sulphate, barium don't move and causes little risk. Barium compounds that are

*Corresponding author.

persistent usually remain in soil surfaces, or at the bottom of water soils [4]. Small amounts of water-soluble barium may cause some diseases such as: difficulties in breathing increase in blood pressures, heart rhythm changes, etc. [4,5].

Strontium compounds can be converted from water insoluble to water soluble by the effect of chemical reaction. The water-soluble compounds cause great damage to human health than the water insoluble ones [6]. Barium forms complexes with other chemicals, like sulfur, carbon or oxygen but strontium is only in strontianite (strontium carbonate) and celestite (strontium sulphate) forms. Hence, a simple method should be explored for their removal before disposing of the wastes in an aquatic system [7]. Chitosan is the N-de-acetylated products of chitin that is the second most plentiful natural biopolymer after cellulose [8]. As an available low-cost adsorbent, this natural polymer and derivatives have received great care in the sorption of metal ions due to the high ratio of hydroxyl groups ($-OH$) and amine groups ($-NH_2$) [9]. The process of chelating resins formation is very important for the collection and separation of metal ions [10]. In the previous work [11], the amidoximated chitosan-grafted polyacrylonitrile was prepared. The authors reported that, the preparation of modified chitosan bearing amidoxime groups (chitosan-g-polyamidoxime) based on graft copolymerization reaction of acrylonitrile onto chitosan to give chitosan-acrylonitrile graft copolymer, and then convert nitrile groups in acrylonitrile side chain of graft copolymer into amidoxime groups. While in the present work, for the first time amino groups in repeating units of chitosan were cyanoethylated via reaction with acrylonitrile to give cyanoethylated chitosan beads as a precursor of chitosan-amidoxime chelating resin (CACR). Different adsorbents were used for adsorption of Ba(II) [3,12–14] and Sr(II) [3,14–21]. In our previous work different prepared chelating resins bearing amidoxime (for adsorption of Cu(II), Ni(II) and Pb(II)), imminodiacetate (for removal of Pb(II), Cd(II), Mn(II) and Zn(II)) and dithiocarbamate groups (for studied its adsorption performance towards Hg(II), Cd(II) and Pb(II)) were reported [22–25]. These chelating resins were prepared starting from synthetic cross-linked polyacrylamide while the chelating resin used in this study was prepared starting from chitosan (natural biopolymer). The aim of the present study is to prepare a new modified chitosan beads with pendent amidoxime moieties and use it for the removal of Ba(II) and Sr(II) from aqueous solution using batch and column techniques. The effects of various parameter like pH value, metal ion concentration, contact time and temperature on adsorption capacity of chelating resin for metal ions will be studied using batch method and will be investigated using Langmuir, Freundlich and Temkin isotherms. Kinetic and thermodynamic parameters of studied metals removal were also estimated. The adsorption performance of CACR toward Ba(II) and Sr(II) using column method will be investigated under different conditions and will be analyzed using Thomas and Yoon–Nelson mathematical models.

2. Materials and methods

2.1. Materials

Chitosan (de-acetylation degree 93%) was purchased from oxford Lab Chem (India), glutaraldehyde (GA),

acrylonitrile (AN), acetic acid (AA), liquid paraffin (LP), hydroxylamine hydrochloride were purchased from Alpha Chemika (India) and were used directly. Metal salts $BaCl_2 \cdot 2H_2O$, $SrCl_2 \cdot 6H_2O$ were pure grade products of Nice Chemicals Pvt.Ltd., (India) were used as sources for Ba(II) and Sr(II), respectively. All the other reagents used in this work were of analytical grade and used as received without purification. De-ionized distilled water was used throughout the experiments.

2.2. Synthesis of cross-linked chitosan beads (CLCB)

Cross-linked chitosan beads were prepared according to the method described by Wang et al. [26]. In brief, 10.0 g of chitosan was dissolved in 200 ml aqueous solution of acetic acid (3%) for 48 h and then added to a 1000 ml beaker flask containing 200 ml of liquid paraffin, continuously stirred for 20 min at 40°C. After that, the temperature was increased to 60°C, and glutaraldehyde was added as the cross-linking agent, continuous stirring at 300 rpm for 3 h to generate the polymeric beads. The resulted beads were washed several times with petroleum ether, ethanol and de-ionized water in sequence to remove any unreacted fraction and dried at 50°C under vacuum for 24 h.

2.3. Synthesis of cyanoethylated chitosan beads (CECB)

Cross-linked chitosan beads (CLCB) (5 g) and acrylonitrile (AN) (50 ml) were mixed in 100 ml methanol then acetic acid (0.2 ml, 99.7%) was added to a flask supported with a magnetic stirrer and reflux. The reaction mixture was stirred at 300 rpm for 48 h and 75°C. After cooling, CECB was filtered, washed several times with ethanol and water and dried at 50°C under vacuum for 24 h.

2.4. Synthesis of chitosan-amidoxime chelating resin (CACR)

A suspension of CECB (5 g) and $NH_2OH \cdot HCl$ (4 g) in 70 ml methanol–water solution (5:1 v/v) was added to a flask equipped with a magnetic stirrer and reflux condenser. About 15 ml of NaOH aqueous solution (7.5 M) was added to this mixture and the pH was kept at 8. The above mixture was stirred for 48 h at 70°C. Finally, the resulted CACR beads was filtered out, washed several times with water and ethanol and dried at 50°C under vacuum for 24 h.

2.5. Characterization of the resin

2.5.1. FTIR analysis

Fourier Transform infrared spectra (FTIR) of the prepared resins were obtained with an FTIR spectrometer (jasco 6100, Japan) in the 400–4000 cm^{-1} range.

2.5.2. Thermal gravimetric analysis

Thermal gravimetric analysis (DSC/TG) for prepared resin (ACCR) was determined using NETZSCH STA 409 C/CD instrument, Germany. The experiment was carried out in a dynamic atmosphere of helium from room temperature to 70°C at heating rate of 10°C/min and a helium flow rate 1 ml/min.

2.5.3. Surface area

Porous structure parameters were characterized by Brunauer–Emmett–Teller (BET) and BJH methods through N_2 adsorption–desorption methods to examine the porous properties of the chelating resin using nitrogen as the adsorbent at 77.35 K. The measurements were performed using a model NOVA 3200 automated gas sorption system (Quantachrome, USA).

2.5.4. Surface morphology and EDX characterization

Scanning electron microscope (SEM) was used to observe the surface morphology of the prepared CACR before and after adsorption of Ba(II) or Sr(II). Micrographs were obtained using SEM model Bruker X-Flash 410M detector attached with Energy Dispersive X-ray (EDX) microanalysis system.

2.6. Adsorption of metal ions

2.6.1. Uptake of metal ions using batch method

All experiments were performed with 0.1 g resin in 250 ml bottles with 100 ml of single metal ion solution on a temperature controlled shaker at 250 rpm. All experiments were carried out at 25°C except the temperature experiments. The desired pH of solution was adjusted using few drops of 0.1 M HCl and 0.1 M NaOH solutions. Concentration of the metal ions in the solution was determined using Perkin Elmer-A Analyst 200 atomic absorption. Experiments were carried out in triplicate. The adsorption capacity was calculated according to Eq. (1).

$$q = \frac{C_o - C_e}{W} \times V(1)$$

where q is the adsorption capacity (mmol/g). C_o and C_e are the initial and the equilibrium concentrations of metal ions (mmol/L), respectively. V is the volume of metal ions solution (L) and W is the weight of dry resin (g). Determination of the optimum pH for adsorption of metal ions, were carried out by shaking 0.1 g of resin with 100 ml (12 mmol/L) metal ion solution for 3 h at adjusted pH.

Experiments of adsorption isotherms were performed by shaking 0.1 g of resin with 100 ml of metal ion solution at optimum pH in a concentration ranging from 1.0 to 18 mmol/L. After 3 h of shaking, the resin was filtered and the remaining metal ion concentration in solution was estimated.

To investigate the adsorption kinetic of the adsorption process, 0.1 g of resin and 100 ml of metal ion solution was continuously shaken at optimum pH and concentration at 25°C. The flasks containing the mixtures were withdrawn at different time intervals to determine the remaining concentration of metal ions.

Measurement of metal ion adsorption by the resin as a function of temperature was studied in the temperature range of 25–55°C. Experiments were performed by shaking 0.1 g of resin with 100 ml of metal ion solutions (1.0 mmol/L) under the optimum pH and contact time. After adsorption, the residual concentration of metal ion was determined as described earlier.

2.6.2. Uptake of metal ions using column technique

A continuous adsorption experiment was carried out in laboratory-scale glass column (17 cm height and 1.2 cm diameter) filled with CACR, forming a homogeneous and well-packed bed. The performance of fixed-bed column was described through a break-through curve and expressed as the ratio of effluent metal ion concentration over influent metal ion concentration (C_{eff}/C_o) as a function of time (t). For optimizing the column dynamic, adsorption experiments were carried out at different bed heights (1.7, 3.4, 5.1 cm), two constant flow rates (0.5, 1 ml/min), 1 mmol/L single metal ion concentration and optimum pH at 25°C. First of all, the column was cleaned by enough de-ionized distilled water in an up flow fashion in order to get rid of air bubbles and to rinse the adsorbent. The remaining concentration of metal ions in the effluent was analyzed as previously described.

The performance of the column adsorption processes is based on the break-through curve which is obtained by plotting C_{eff}/C_o vs time (t), where C_{eff} and C_o are effluent and influent metal ion concentration (mmol/L), respectively. The mass transfer zone (Δt) [27] is given by Eq. (2)

$$\Delta t = t_e - t_b \quad (2)$$

where t_b is the break-through time (which is the time needed for the increase of metal ion concentration in the effluent to an appreciable value in a sudden way) and t_e is the bed exhaustion time (which is the time needed for the increase of metal ion concentration in the effluent exceeding 99% of the influent concentration).

The length of the mass transfer zone (Zm) [28] is obtained from the break-through curve and is calculated from Eq. (3)

$$Zm = Z \left(1 - \frac{t_b}{t_e} \right) \quad (3)$$

where Z is the bed height in mm. The total column adsorption capacity (q_{total}) [28] is calculated from Eq. (4).

$$q_{total} = \frac{QA}{1000} = \frac{Q}{1000} \int_{t=0}^{t=t_{total}} (C_{ad}) dt \quad (4)$$

where A is the area under the break-through curve of the plot between C_{ad} ($C_{ad} = C_o - C_{eff}$) versus time, Q is the flow rate (ml/min) and t_{total} is the total flow time (min). The equilibrium adsorption capacity (q_e) (mmol/g) [27] is calculated by Eq. (5).

$$q_e = \frac{q_{total}}{m} \quad (5)$$

where m is the total dry weight of CACR (g). The total amount of metal ions fed to the column is calculated from Eq. (6) [28].

$$W_{total} = \frac{C_o Q t_{total}}{1000} \quad (6)$$

where W_{total} is the whole amount of metal ion placed inside the column. Total percentage removal of metal ions is calculated from Eq. (7) [28].

$$\text{Percentage removal (\%)} = \frac{q_{\text{total}}}{W_{\text{total}}} \times 100 \quad (7)$$

Elution experiments were carried out by placing 1.0 g of CACR in the column then loaded with Ba(II) or Sr(II) at flow rate of 0.5 mL/min. The maximum uptake was obtained in the first run, there after the adsorbent was washed by flowing distilled water crossing the column. The synthesized adsorbent loaded by Ba(II) or Sr(II) was subjected for elution by using 2 M HNO₃. After treating CACR with the eluent, it was washed carefully with diluted solution of NaOH and double distilled water to become ready for reuse for the second run of adsorption.

3. Results and discussion

3.1. Synthesis of CACR

According to this research study, CACR was prepared via modification process of chitosan according to the following three steps presented in Fig. 1. The first step represents cross linking reaction of chitosan beads using glutaraldehyde as cross linking agent to give CLCB, the second step illustrates cyanoethylation reaction of remaining amino groups of CLCB via reaction with acrylonitrile to give CECB. It is worth mentioning here for the first time amino group in repeating unit of chitosan has been cyanoethylated. The final step is reaction of chitosan beads supported nitrile group with NH₂OH·HCl to convert nitrile groups into amidoxime groups, forming CACR.

3.2. Characterization of the synthesized resin

3.2.1. FT-IR analysis

Fourier Transform Infrared absorption spectra of chitosan, CLCB, CECB and CACR were illustrated in Fig. 2. Fig. 2a shows spectrum of pure chitosan, the –OH and –NH₂ (stretching vibration) groups are presented at peak

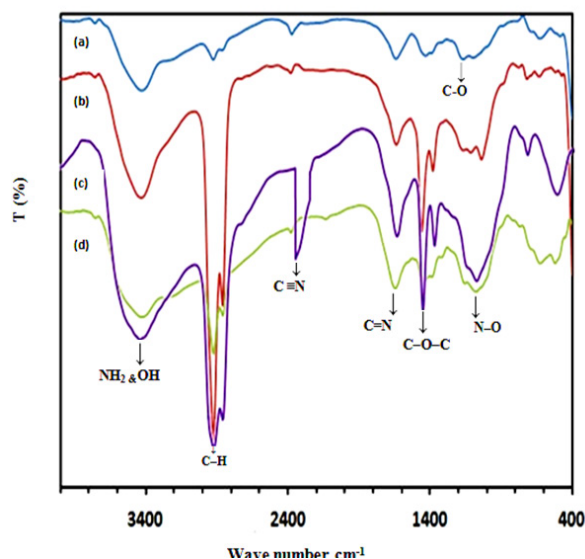


Fig. 2. FTIR spectra of (a) pure chitosan (b) CLCB, (c) CECB and (d) CACR.

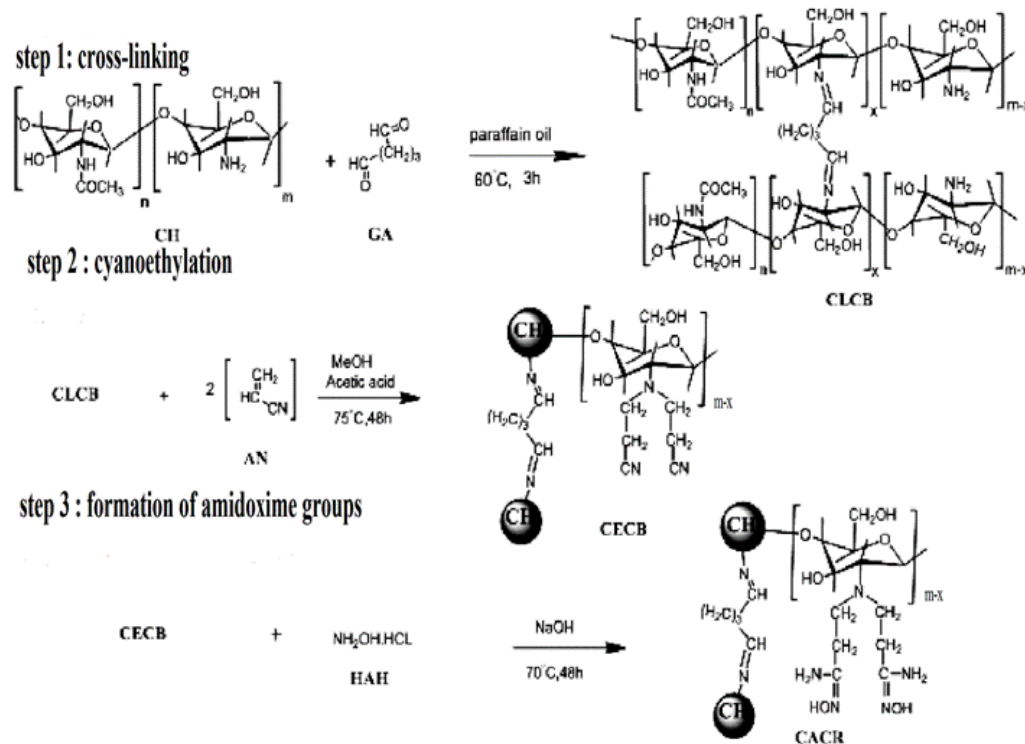


Fig. 1. Preparation steps of CACR.

3427.85 cm^{-1} (broad band). The C–O–C bridge absorption band (asymmetric stretching) was observed at 1165.76 cm^{-1} , while skeletal vibration of C–O stretching corresponds to the bands at 1095.37 and 1041.37 cm^{-1} [29]. FT-IR spectrum of CLCB (Fig. 2b) illustrates stretching vibration bands of C–H (symmetric and asymmetric) which enlarges at 2923.56 and 2858.95 cm^{-1} and the peak at 1637.27 cm^{-1} is seen due to imine bonds C=N [30–32]. After reaction with acrylonitrile, a new absorption band appears at 2252.45 cm^{-1} which is characteristic of the nitrile vibration band as shown in Fig. 2c. Finally FTIR spectrum of CACR (Fig. 2d) revealed that the absorption band of the $-\text{C}\equiv\text{N}$ group at 2252.45 cm^{-1} disappears and a new band at 1075.12 cm^{-1} appears due to the vibration absorption of the N–O bond in the amidoxime group [33].

3.2.2. Thermal gravimetric analysis (TGA) of CACR

TGA was applied to illustrate the thermal stability of the chelating resin. The thermo-gram of the CACR is presented in Fig. 3 and Table 1. The TGA curve indicates that CACR undergoes degradation in five steps. The first degradation stage ranges from 26 to 220°C with partial weight loss of 19.73% attributable to loss of water molecules which is present in outside surface and internal pores or cavities of the resin. The higher water content ensures the hydro-

philic property of the resin. The 2nd stage ranges from 220 to 280°C with partial weight loss 32.64%. As shown in Fig. 3 the continuity of heating until 700°C trends to gradual loss of weight which finally reached 6.70%.

Differential scanning calorimeter (DSC) is an excellent tool to measure the thermal stability of the CACR at different temperatures. This device allows quick and accurate results for the thermal stability. The DSC is a direct examination for various heat up-takes between an inert (He) gas as reference and a sample. Five stages heating process were conducted for the DSC analysis in Fig. 4. As shown in Table 1 the first stage heating is used to decrease the water content inside the resin and showed endothermic peak at 204.5°C which indicates the high stability of CACR and its ability to acquire more heat energy.

Four other endothermic peaks are shown in Fig. 4 due to the continuous heating which represents a large scale, ensures the high stability of CACR as thermal decomposition of resin starts after 509.2°C and there was a trend to total thermal decomposition presented in flat line.

3.2.3. Scanning electron microscope (SEM–EDX)

The surface morphology of CACR was examined by scanning electron microscopy and energy dispersive X-ray microanalysis (EDX) system. The scanning electron micro-

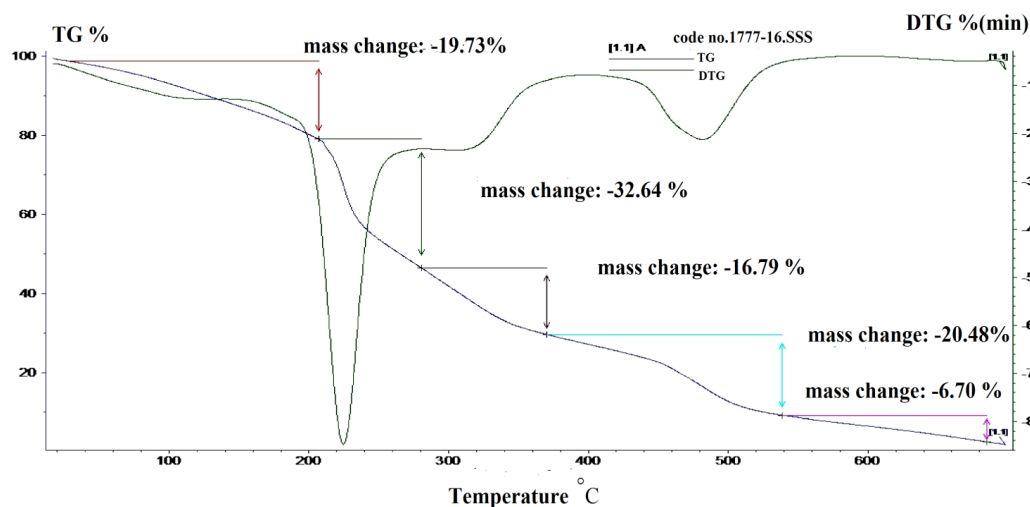


Fig. 3. TGA for CACR.

Table 1
TGA and DSC Analysis of CACR

TGA	1 st	2 nd	3 rd	4 th	5 th
	degradation step (°C)				
	26–220	220–280	280–370	370–540	540–700
DSC	1 st	2 nd	3 rd	4 th	5 th
	Endothermic peak (°C)				
	204.5	211.5	225.8	457.5	509.2

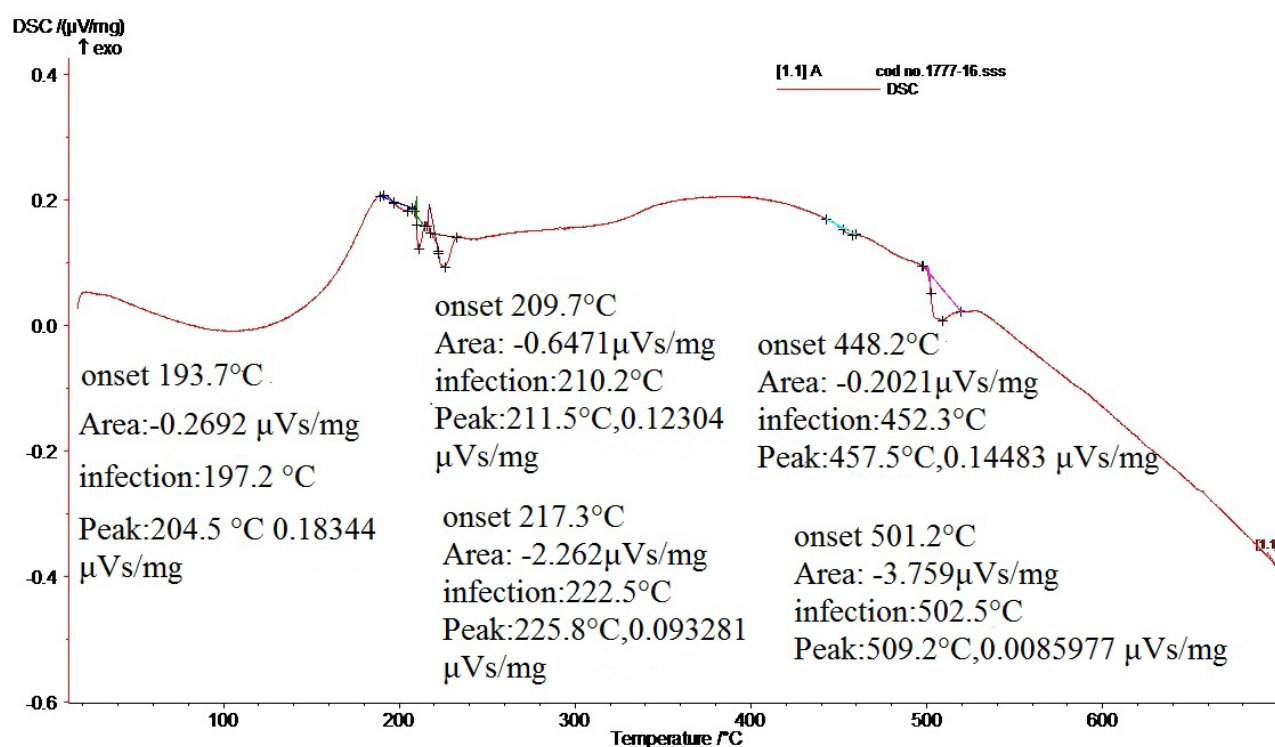


Fig. 4. DSC for CACR.

graph images of CACR, CACR-Ba(II) and CACR-Sr(II) are shown in Fig. 5a–c, respectively. The morphology of CACR before metal ion uptake shows clear empty cavities which can help for mass transfer of metal ions to its surface. After metal ion uptake, the resin surface became totally saturated and the cavities disappeared specially in CACR-Ba(II), this means that barium ions have high adsorption rate than that of strontium ions, which still contains unfilled cavities. The presence of barium and strontium in the synthesized CACR was confirmed from Energy dispersive X-ray spectroscopy (EDX) measurements (Fig. 6). CACR-Ba(II) shows new distinct signals at 0.5 and 4.5 keV corresponding to Ba while CACR-Sr(II) shows new signal at 1.9 keV corresponding to Sr. The aim of this analysis was to map elemental Ba and Sr qualitatively (not quantitatively) on the composite surface. However, the level of the Ba(II) and Sr(II) signals observed was sufficient for providing a quantitative idea of the homogeneous distribution of Ba and Sr elements at the surface of the sorbent, the percentage (in mass) of Ba(II) and Sr(II) was 31.35% and 12.07%, respectively.

3.2.4. Surface area

Before examination, the resin was put in vacuum at 300°C for 2 h by means of adsorption of ultra-pure nitrogen at 77.35 K. The surface area was measured using the Brunauer–Emmett–Teller (BET) and BJH method based on adsorption data in the partial pressure (P/P^0) range of 0.09–0.29. The total pore volume was determined from the amount of nitrogen adsorbed at $P/P^0 = 0.29729$. Pore size

and pore volume were collected in Table 2. These results show that the resin has surface area of 39.52 m²/g with pore diameter of 2.981 nm which to be considered mesoporous structure and lead to efficient transfer the metal ions to the internal adsorption sites.

3.3. Uptake of metal ions by batch technique

3.3.1. Optimum pH of metal ions uptake

The influence of the pH on the uptake capacity of metal ion was examined by batch system at 25°C in the pH range of 1.0–9.0 and the results were presented in Fig. 7. The amidoxime group ($-C(NH_2)=N-OH$), has amphoteric property [34]. At lower pH value, the basic amino group ($-NH_2$) lose the ability to make complex with metal ions M(II) since ($-NH_2$) group blocked and give ($-NH_3^+$), that cause the decrease in metal ion uptake. By increasing pH value, the concentration of H⁺ ions decreased therefore protonation of ($-NH_2$) group will be weakened which cause high chelation of amino group toward metal ions. Also, the level of dissociation of ($-OH$) group will increase and give ($-O^-$) resulting in electrostatic interaction between amidoxime groups of CACR and metal ions, leading to high metal ion sorption. As presented in Fig. 7, the adsorption capacity increases when the pH value was increased until it reaches the maximum (optimum value). The optimum pH value which resulted in the greatest adsorption capacity for metal is located at 7.0 and 8.5 for Ba(II) and Sr(II), respectively. Consequently, for this work all the consequent experiments were performed at these optimum pH values. Above these

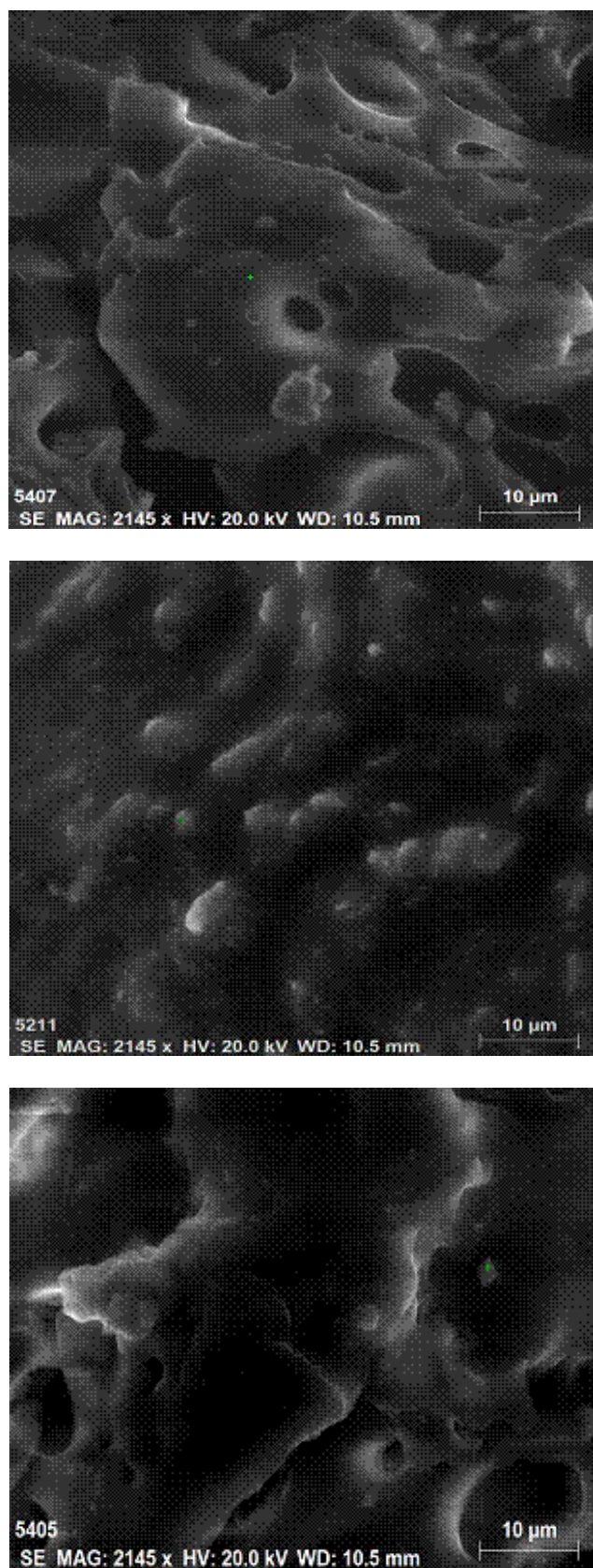


Fig. 5. SEM micrographs of (a) CACR, (b) CACR-Ba and (c) CACR-Sr.

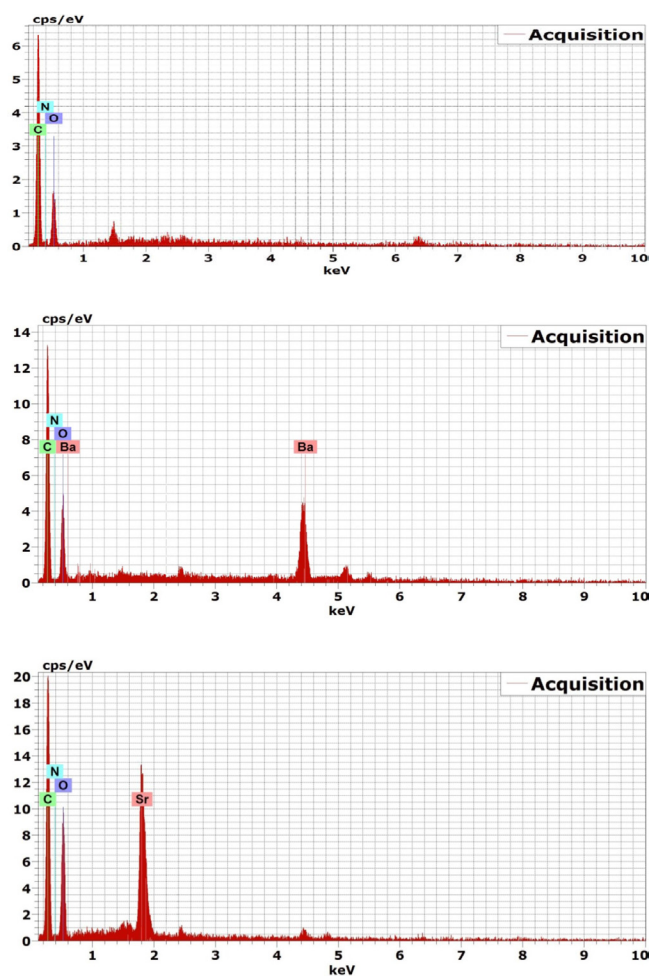


Fig. 6. EDS of (a) CACR, (b) CACR-Ba and (c) CACR-Sr.

Table 2
Porous structure parameters of CACR.

Parameters	CACR
BET surface area (m^2/g)	39.52
BJH desorption average pore diameter (nm)	2.981
BJH desorption cumulative volume of pores (cm^3/g)	0.1405

optimum pH, metal is converted to precipitated metal(II) hydroxide and the adsorption of these ions cannot be measured accurately. The possible chelation model of CACR with metal ions is shown in Fig. 8.

3.3.2. Effect of initial concentration and equilibrium isotherm models

The influence of the initial metal ion concentrations on equilibrium adsorption was studied and the results are illustrated in Fig. 9. The results showed that the amount of Ba(II) and Sr(II) adsorbed onto CACR increased as the ini-

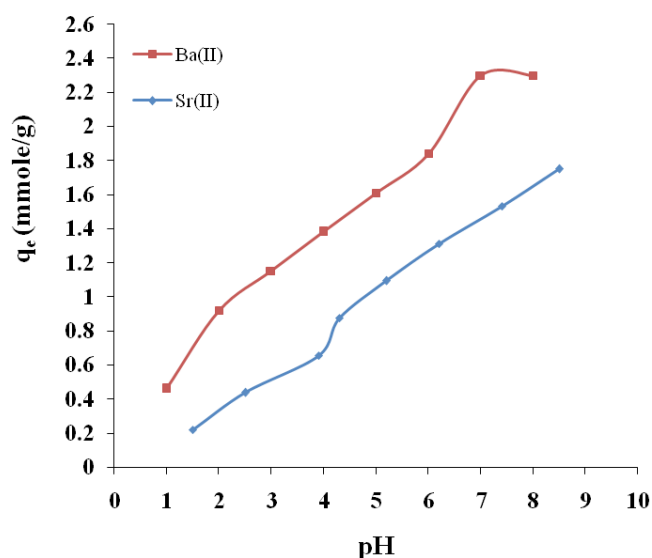


Fig. 7. Effect of pH on the uptake of metal ions at 25°C; shaking time, 3h and initial metal ion concentration of 12 mmol/L.

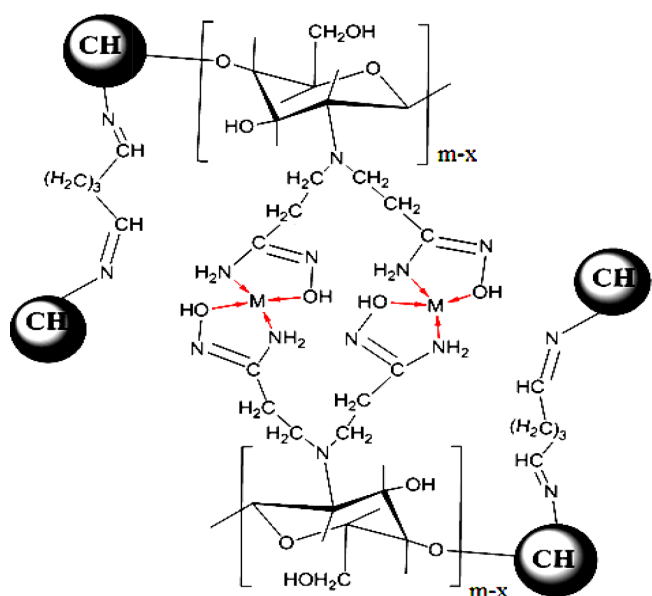


Fig. 8. Chelation of CACR for metal ions.

tial concentration of metal ions increased before reaching a plateau shape. The maximum adsorption capacity was obtained at optimum pH of each metal ion and at 25°C and illustrated in Table 3. The results showed that the maximum adsorption capacity of Ba(II) and Sr(II) reached 2.30 and 1.75 mmol/g, respectively at maximum initial concentration of 12 mmol/L. These differences in metal ions uptake are possibly related to the difference in hydrated ionic radius of these ions. Hydration of an ion is directly proportional with the electrostatic attraction of water molecule to that ion. Because attraction of water molecules around an ion depends on that ion's density of charge, ions of smaller size (and thus ions of greater ionic poten-

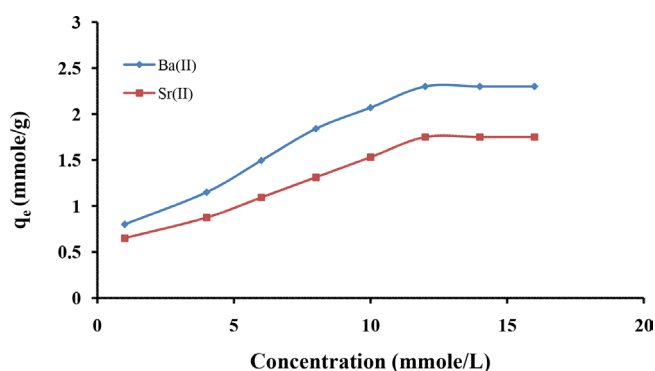


Fig. 9. Effect of initial metal ions concentration on the adsorption capacity of Ba(II) and Sr(II); 25°C; shaking time 3 h and at the optimum pH value.

tial) attract more water molecules. So there is an inverse relationship between non-hydrated radius and hydrated radius. The hydrated ionic radius of these metal ions is in the order of Ba(II) (1.5 Å) < Sr(II) (1.8 Å) [35]. This means that the smaller the hydrated ionic radius, the higher the amount of metal ions adsorbed. Ba(II) was adsorbed more than Sr(II) by CACR (Fig. 9) because of its smaller hydrated ionic radius since it is easily taking place in the pores of chelating resin (average pore diameter of CACR equal to 2.98 nm). A comparison of the present CACR with those of various types of adsorbents in other reported literatures is listed in Table 3. The data presented in Table 3 reveals that, generally, the prepared CACR in this work has a good advantage in metal ion adsorption compared to the previously reported adsorbents except the adsorbent of modified silica gel with crown ether [16].

Equilibrium isotherm data were analyzed using Langmuir, Freundlich, and Temkin isotherm models. The Langmuir isotherm model is based on the adsorption of the mono layer of metal ions onto a homogenous surface of the chelating resin. The linear form of Langmuir adsorption model is represented as [36]:

$$\frac{C_e}{q} = \frac{C_e}{Q_{\max}} + \frac{1}{KQ_{\max}} \quad (8)$$

where C_e is the equilibrium concentration of metal ions (mmol/L), q is the equilibrium adsorption capacity (mmol/g), Q_{\max} (mmol/g) and K (L/mmol) are the maximum adsorption capacity and binding constant, respectively. The parameters of Langmuir model are listed in Table 4. Langmuir isotherm model also defined in terms of the dimensionless parameter known as separation factor (R_L) [37] which is represented as follows:

$$R_L = \frac{1}{1 + KC_0} \quad (9)$$

where K is the Langmuir constant (binding constant) and C_0 is the initial concentration of metal ion (mmol/L). The value of R_L which is calculated recommends the shape of the isotherm to be unfavorable ($R_L > 1$), linear ($R_L = 1$), favorable ($0 < R_L < 1$), or irreversible ($R_L = 0$) [38,39]. Plotting R_L vs. C_0 is shown in Fig. 10. The calculated values of R_L were between zero and one for all metal ions revealed that the

Table 3
Comparison of maximum adsorption behavior of synthesized CACR among different adsorbents reported in literature for the adsorption of Ba(II) and Sr(II)

Adsorbents	Metal ions	Sorption capacity (mmol/g)	Conditions	Ref.
Expanded Perlite(EP)	Ba(II) and Sr (II)	0.02 and 0.01	pH=6 and 20°C	[3]
Chelating Agent	Ba (II)	0.08	pH=2.2 and 25°C	[12]
maghemite and titania nanoparticles in PVA and alginate beads	Ba(II)	0.14	pH = 8.0 and 25°C	[13]
Dolomite Powder	Ba(II) and Sr(II)	0.03 and 0.01	pH= 5.5 and 20°C	[14]
Prussian blue analog caged in chitosan surface-decorated carbon nanotubes	Sr(II)	2.34	pH= 6 and 20 ± 2°C	[15]
novel silica-based 4,4i ,(5i)-di(tert-butylcyclohexano)-18-crown-6 extraction resin	Sr (II)	5.189	pH=2 and 25°C	[16]
Porous Chelating Polymers	Sr (II)	2.15	pH=9 and 25°C	[17]
Scenedesmus spinosus	Sr (II)	0.03	pH=6.5-7 and 25°C	[18]
Activated Zeolite	Sr(II)	0.84	pH=1 and 25°C	[19]
activated porous calcium silicate	Sr(II)	1.50	pH = 7.0 and 15°C	[20]
Zeolite A	Sr(II)	1.04	pH = 6.0 and 25°C	[21]
CACR	Ba(II) and Sr (II)	2.30 and 1.75	pH = 7 , 8.5 and 25°C	This work

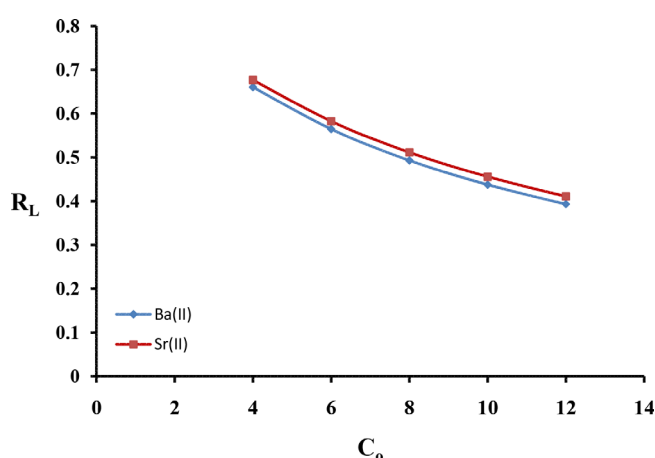


Fig. 10. Variation of adsorption intensity (R_L) with initial metal ion concentration (C_o).

metal ion adsorption onto CACR is favorable. As indicated in Fig. 10, the R_L values decreased as the (C_o) of metal ions increased which showed that the adsorption of metal ions is more effective at higher initial concentration.

The Freundlich isotherm model is an empirical equation which refers to a heterogeneous adsorption system.

The Freundlich isotherm model is shown by the following equation [40]:

$$\log q = N \log C_e + \log K_F \quad (10)$$

where q is the equilibrium adsorption capacity (mmol/g), C_e is the equilibrium concentration of metal ion (mmol/L), K_F and N are the Freundlich constants for the adsorption capacity (mmol/L) and a measurement of efficiency of adsorption, respectively. The values of K_F and N were calculated and collected in Table 4.

Like R_L values that values of term N presents the nature of isotherm to be unfavorable ($N > 1$), favorable ($0 < N < 1$) or irreversible ($N = 0$). The values calculated for N ranges between (0) and (1) for all metal ions which refers to the simplicity of adsorption process of metal ions onto chelating resin.

The Temkin isotherm model is expressed by the following equation [41]:

$$q = B \ln K_T + B \ln C_e \quad (11)$$

where B and K_T are Temkin constants which represent the heat of adsorption and equilibrium binding constant, respectively. B and K_T are tabulated in Table 4.

Table 4
The parameters of Langmuir, Freundlich and Temkin isotherms for CACR at 25°C

Metal ion	Langmuir isotherm			Freundlich isotherm			Temkin isotherm		
	Q_{\max}	K	R^2	N	K_F	R^2	K_T	B	R^2
Ba(II)	4.065	0.1285	0.994	0.580	0.612	0.997	1.065	0.959	0.994
Sr(II)	3.125	0.1194	0.958	0.574	0.457	0.994	1.044	0.716	0.969

As shown in Table 4, the good fit experimental data with Langmuir, Freundlich, and Temkin isotherm models and high correlation coefficient (R^2) obtained for these plots indicates the validity of these models to CACR for both metals ions. But Freundlich equation shows better results than Temkin and Langmuir models because of higher correlation coefficient for both metal ions.

3.3.3. Effect of contact time on adsorption process

In order to determine the influence of contact time between CACR and aqueous solution of Ba(II) and Sr(II) ions adsorption, variations of adsorption capacity (q_e) vs. time (15–300 min) are plotted in Fig. 11. It was found that, the adsorption of Ba(II) and Sr(II) ions from aqueous solution using the adsorbent is continuously increased with time increase until reaching equilibrium between two phases after 3 h. Therefore, this optimum equilibrium time was selected for the next adsorption experiment.

The adsorption results were used to investigate the kinetic mechanism which controls the adsorption process. The most widely used models of Lagergren's pseudo-first order; pseudo-second order and intra particle diffusion were used to investigate the kinetic process [42–44].

The linear form of the first order rate equation by Lagergren and Svenska [42] is expressed in Eq. (12):

$$\text{Log}(q - q_t) = \text{log } q - \left(\frac{K_{ads}}{2.303} \right) t \quad (12)$$

where q and q_t are the adsorption capacity (mmol/g) at equilibrium and at time t (min), respectively. K_{ads} is the Lagergren rate constant (min^{-1}) of the adsorption.

Plots of Eq. (12) were made for Ba (II) and Sr(II) ions sorption at different times. Lagergren constants are listed in Table 5.

The experimental data were also treated according to pseudo-second order kinetic model. The pseudo-second order model of Ho [43] can be expressed in the linearized form as follows:

$$\frac{t}{q_t} = \frac{1}{K_2 q^2} + \left(\frac{1}{q} \right) t \quad (13)$$

where K_2 ($\text{g mmol}^{-1} \text{min}^{-1}$) is the pseudo-second order rate constant. The constants of the second order kinetic model plots are given in Table 5. Obviously, as it can be seen from the result listed in Table 5, correlation coefficient values (R^2) of the second order kinetic are higher than the values obtained from the first-order kinetics. Therefore, the sorption behavior of Ba(II) and Sr(II) onto CACR obeys the second-order kinetics.

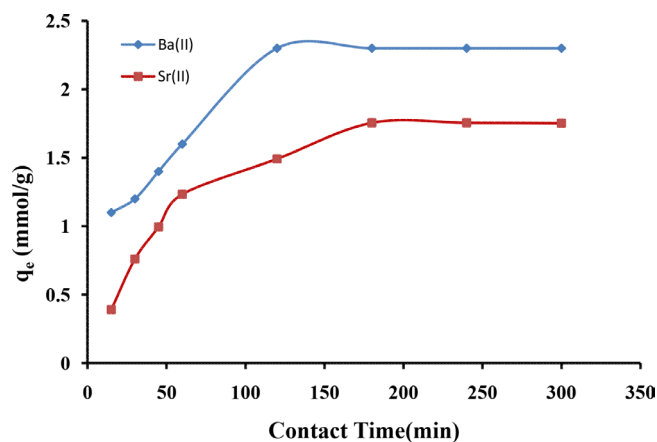


Fig. 11. Effect of contact time on the amount of sorbent of Ba(II) and Sr(II) ions on CACR at 25°C, 12mmol/L and optimum pH.

Intraparticle diffusion model is described using Eq. (14) proposed by Weber and Morris [44].

$$q_t = K_{id} t^{0.5} \quad (14)$$

where K_{id} is the intraparticle diffusion rate constant ($\text{mmol g}^{-1} / \text{min}^{0.5}$). K_{id} was determined from the plot of q_t against $t^{0.5}$ (Fig. 12). The constants of these plots are listed in Table 5. According to Weber and Morris, the adsorbate could be transported from the aqueous phase over adsorbent in three different steps as: (a) Diffusion of metal ions through the boundary layer to the surface of the chelating resin; (b) Intra-particle diffusion: migration of metal ions from the outside surface of the chelating resin to the inside holes or pores of the resin through a pore diffusion or intra-particle diffusion mechanism; and (c) Adsorption of metal ions in an active area on the surface of chelating resin by the effect of chelation.

With respect to Eq. (14), if the plot gives a straight line, intra-particle diffusion is accepted as the only rate-limiting step, but multi-linearity is formed which refers to two or more stages related to the adsorption of metal ions [45]. The adsorption process was restricted by three stages: (1) rapid transportation of metal ions from solution to the resin surface (2) gradual adsorption stage where intra-particle diffusion is rate-limiting step, and (3) final equilibrium stage where intra-particle diffusion begins to slow due to the very low metal ion concentration in the solution, in addition to fewer number of adsorption areas are available. Based on these results, we can conclude that the intra-particle diffusion is not the only step of rate control. This behavior recommends that adsorption processes involve more than one single kinetic stage.

Table 5
First-order, second-order and intra particle diffusion rate constants

Equations	Parameters	Ba(II)	Sr(II)
Pseudo-first order kinetic equation	q(mmol/g)	1.499	1.555
	K_{ads} (1/min)	0.011	0.014
	R^2	0.960	0.975
Pseudo-secondorder kinetics	q(mmol/g)	2.577	2.127
	K_2 (gmmol ⁻¹ min ⁻¹)	0.600	0.184
	R^2	0.993	0.992
Intraparticle diffusion equation	K_{id} (mmol g ⁻¹ min ^{-1/2})	0.101	0.098
	R^2	0.863	0.885

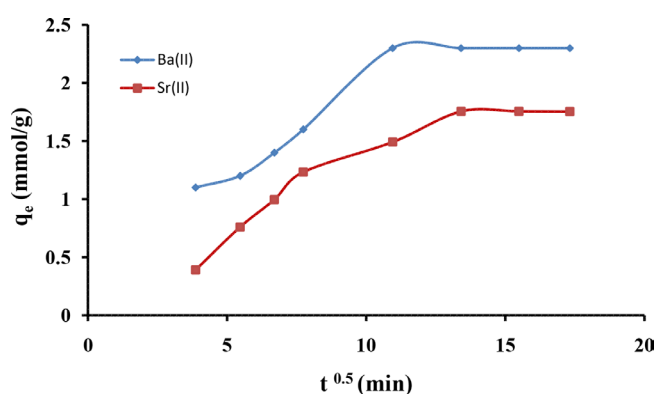


Fig. 12. Plot of Weber-Morris intra particle diffusion models for the adsorption of Ba(II) and Sr(II) ions on CACR at 25°C.

3.3.4. Adsorption thermodynamics parameters

Thermodynamic parameters of the adsorption process were examined by performing the adsorption experiments at different temperatures (25, 35, 45 and 55°C). Metal ion solution (100 ml, 1.0 mmol/L) equilibrated with 0.1 g of CACR at optimum pH value.

Equilibrium distribution coefficient (K_d) for the adsorption process was calculated by Eq. (15) [46].

$$K_d = \frac{C_o - C_e}{C_e} \times \left(\frac{V}{W} \right) \quad (15)$$

where C_o and C_e are the initial and equilibrium concentration of the metal ions in aqueous solution, respectively (mmol/L), V is the total volume of the solution (L) and W is the weight of the CACR (g).

Free energy change of the adsorption (ΔG_{ads}°) was calculated using the following equation:

$$\Delta G_{ads}^\circ = -RT \ln K_d \quad (16)$$

The standard enthalpy change (ΔH_{ads}°) and entropy change (ΔS_{ads}°) of the adsorption were estimated by plotting $\ln K_d$ versus $1/T$ according to Eq. (17).

$$\ln K_d = \frac{\Delta S_{ads}^\circ}{R} + \frac{\Delta H_{ads}^\circ}{RT} \quad (17)$$

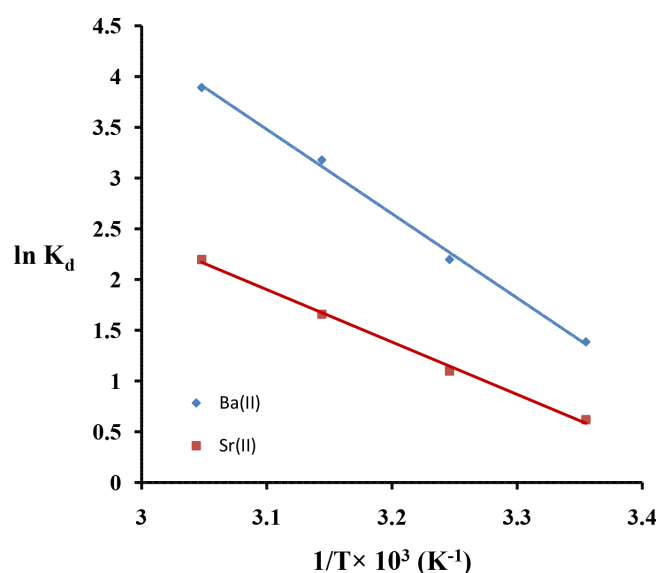


Fig.13. Plot of $\ln K_d$ as a function of reciprocal of temperature ($1/T$) for the adsorption of metal ions on CACR.

where R is gas constant (8.314 J/mol K). The values of the slope and the intercept (Fig. 13) give ΔH_{ads}° and ΔS_{ads}° respectively. Thermodynamic parameters involving ΔG_{ads}° , ΔH_{ads}° and ΔS_{ads}° for metal ion adsorption onto CACR are illustrated in Table 6. As it can be seen from Table 6, Positive values of ΔH_{ads}° shows that the metal ion adsorption is an endothermic process [47,48]. Also, the positive values of ΔS_{ads}° may be correlated with the increased randomness due to the liberation of H_2O of hydration during the adsorption of metal ions [47,48]. Finally, the thermodynamic parameters showed that there is continuity in adsorption process that is indicated by negative values of ΔG_{ads}° .

3.4. Uptake of metal ions using column technique

The break-through curves (C_{eff}/C_o vs. time) were obtained for Ba(II) and Sr(II) sorption onto CACR at different bed depth (1.7, 3.4, 5.1 cm), two constant influent flow rates (0.5, 1 ml/min) and 1 mmol/L single metal ion concentration. The break-through curves are shown in Figs. 14 and 15. The

Table 6
Thermo-dynamic parameters for the adsorption of metal ions onto CACR

Metal ion	$-\Delta G_{\text{ads}}^{\circ}$ (kJ/mol)				$\Delta H_{\text{ads}}^{\circ}$ (kJ/mol)	$\Delta S_{\text{ads}}^{\circ}$ (J/mol)	R^2
	298K	308K	318K	328K			
Ba(II)	3.43	5.63	8.40	10.61	69.047	242.9	0.997
Sr(II)	1.53	2.81	4.38	5.99	42.958	148.9	0.996

Table 7
Column data parameters, Thomas and Yoon Nelson Models constants at different flow rates and bed heights ($C_0 = 1$ mmol/L)

Metal ion	Q (mL/min)	Z (cm)	Calculated parameters			Thomas model				Yoon Nelson model		T_{exp} (min)	
			q_{total} (mmol)	q_e (mmol/g)	R %	Zm (cm)	q_e (mmol/g)	K_{th} (L/mmole-min)	R^2	K_{YN} (min ⁻¹)	T min		R^2
Ba(II)	0.5	1.7	0.2070	0.2070	68.98	1.055	0.2179	0.01924	0.9947	0.01924	436	0.9947	434
	0.5	3.4	0.3002	0.1501	75.03	1.830	0.1561	0.01638	0.9938	0.01638	624	0.9938	629
	0.5	5.1	0.4334	0.1444	77.38	2.318	0.1479	0.01729	0.9919	0.01729	888	0.9919	890
	1	1.7	0.1538	0.1538	64.07	1.108	0.1650	0.04300	0.9950	0.04300	165	0.9950	165
	1	3.4	0.2220	0.1111	76.55	1.821	0.1182	0.04112	0.9958	0.04112	236	0.9958	239
	1	5.1	0.3218	0.1073	78.48	2.423	0.1112	0.03853	0.9891	0.03853	334	0.9891	333
Sr(II)	0.5	1.7	0.1193	0.1193	56.80	1.190	0.1301	0.01980	0.9963	0.01980	260	0.9963	254
	0.5	3.4	0.1698	0.0849	62.88	2.090	0.0900	0.02011	0.9888	0.02009	360	0.9888	360
	0.5	5.1	0.2534	0.0845	66.68	3.440	0.0894	0.01456	0.9703	0.0146	537	0.9703	523
	1	1.7	0.0776	0.0776	51.72	1.214	0.0873	0.05815	0.9915	0.05815	87	0.9915	88
	1	3.4	0.1029	0.0515	57.16	2.200	0.0569	0.05011	0.9877	0.05011	114	0.9877	112
	1	5.1	0.1356	0.0452	64.55	2.805	0.0491	0.04871	0.9856	0.04871	147	0.9856	144

mass transfer zone (Z_m), the sorption capacity of CACR (q_e) and removal percentage ($R\%$) were calculated from the break-through curves by using Eqs. (2)–(7) and presented in Table 7. According to results, CACR showed a higher adsorption capacity for Ba(II) than Sr(II). The maximum sorption capacity was about 0.2070 and 0.1193 mmol/g for Ba(II) and Sr(II), respectively, at flow rate of 0.5 ml min⁻¹ and bed height of 1.7 cm, which corresponds to 68.98% and 56.80% for Ba(II) and Sr(II) removal, respectively.

3.4.1. Effect of bed height

The break-through curves of sorption of Ba(II) and Sr(II) are shown in Figs. 14 and 15. As shown in Figs. 14 and 15 the shape of break-through curves of sorption of Ba(II) and Sr(II) at both 0.5 and 1 ml min⁻¹ flow rates are significantly different as depth changed from 1.7 to 5.1 cm. It was observed that the break-through time and exhaustion time were increased with increased in bed heights [49,50]. This may be due to the amount of resin was more to contact with Ba(II) and Sr(II) metal ions. At higher bed heights a larger volume of metal solution could be treated as shown in Table 7 due to increase in the ratio of the resin where more active binding areas are available for processing the sorption process. The break-through time t_b , exhaustion time t_e , the height

of mass transfer zone (Z_m) and percentage removal ($R\%$) increased with rise in bed height. The increase in percentage removal must be related to the maximum saturation of all active sites in the adsorbent dosage by metal ions and broad ended mass transfer zone. The decreasing of uptake capacities by increasing the bed height is due to the change in volume to mass ratio [51,52].

3.4.2. Effect of flow rate

It was observed that the column performance is very well at lower flow rate. At higher flow rate, the break-through time and exhaustion time reached more rapid and this may be due to the inadequate residence time of the metal ion of Ba(II) and Sr(II) with the resin [53]. The result reveals that the break-through curve becomes steeper as the flow rate increased. The metal sorption capacity decreases with increase in flow rate (Table 7). This is because a much longer time is needed between the solute and that of the solid phase to reach equilibrium state. Therefore, this increase in flow rate causes a shorter presence time of the solute in the column and so, the metal ion leaves the column before equilibrium occurs [54]. Hence break-through time, bed exhaustion time, and sorption capacity were more at 0.5 ml min⁻¹ when compared to 1 ml min⁻¹ flow rate.

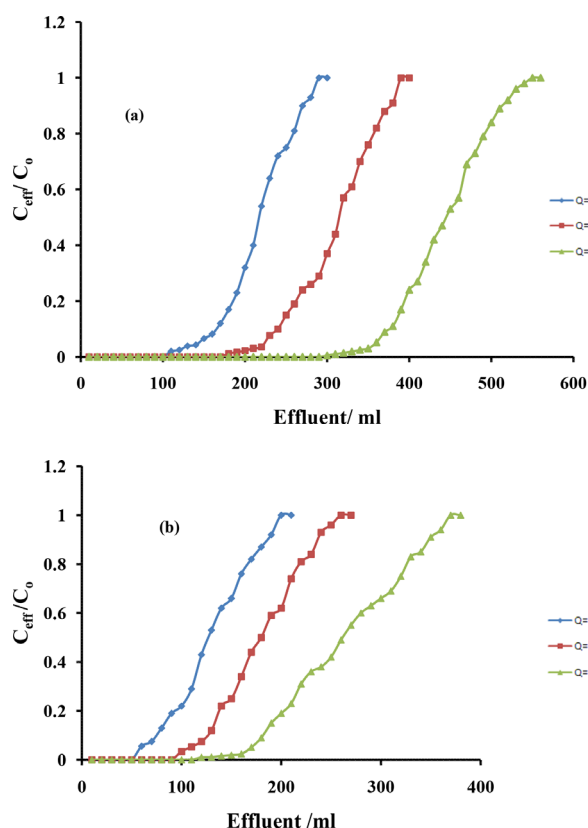


Fig. 14. Break-through curves for (a) Ba(II) and (b) Sr(II); initial concentration is 1.0 mmol/l, flow rate is 0.5 ml/min at optimum pH and at 25°C and bed depth (1.7, 3.4, 5.1cm).

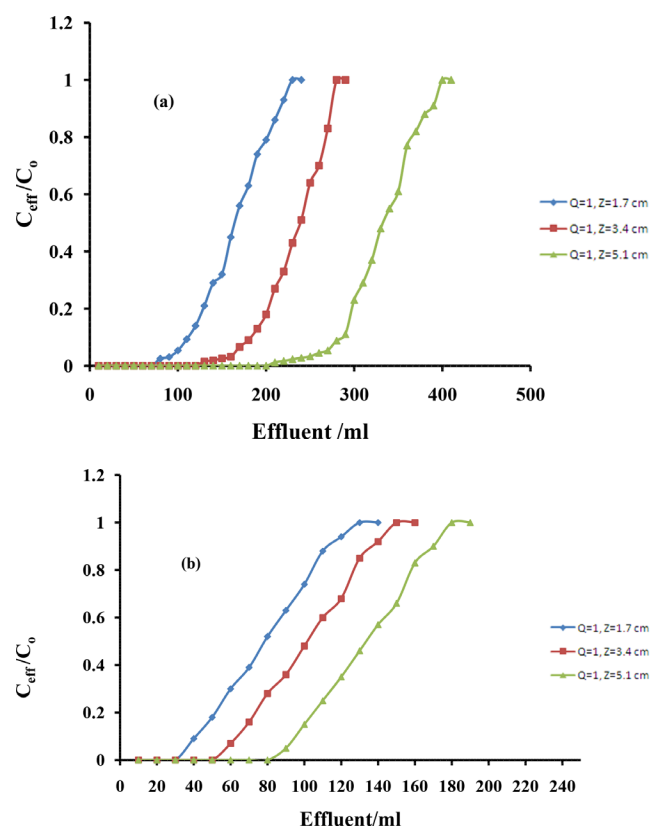


Fig. 15. Break-through curves for (a) Ba(II) and (b) Sr(II); initial concentration is 1.0 mmol/l, flow rate is 1 ml/min at optimum pH and at 25°C and bed depth (1.7, 3.4, 5.1cm).

3.4.3. Modeling of column experimental data

Various theoretical models such as Thomas and Yoon-Nelson models [54–56] were tested to show the experimental data related to the solute interaction behavior and to estimate the break-through curves.

3.4.3.1. Thomas model

The obtained data from the experiments were used to measure the adsorption capacity of CACR and the adsorption rate constant using Thomas model based on Eq. (18).

$$\frac{C_{eff}}{C_o} = \frac{1}{1 + \exp\left[\frac{K_{Th}q_e m}{Q} - \frac{K_{Th}C_o V_{eff}}{Q}\right]} \quad (18)$$

where K_{Th} is the Thomas rate constant (l/mmol-min), m is the total dry weight of CACR(g), V_{eff} is effluent volume, q_e adsorption capacity of Ba(II) and Sr(II) ions on CACR (mmol/g). The linearized form of Thomas model is given by Eq. (19).

$$\ln\left(\frac{C_o}{C_{eff}} - 1\right) = \left[\frac{K_{Th}q_e m}{Q} - \frac{K_{Th}C_o V_{eff}}{Q}\right] \quad (19)$$

To detect maximum adsorption capacity of the adsorbent (q_e) and kinetic coefficient (K_{Th}) in Thomas model, experimental data were fit into Eq. (19). This equation was used to fit the experimentally obtained data by plotting $\ln((C_o/C_{eff}) - 1)$ against the effluent volume. The Thomas rate constant and the ion exchange capacity were determined from the slope and intercept, respectively. The values of these two parameters are given in Table 7 for Ba(II) and Sr(II) at 10% saturation. According to Table 7 the calculated q_e from Thomas model is similar to the experimental q_e and the value of q_e decreased with increasing both flow rate and bed height. As can be observed, the experimental data are in good agreement with theoretical results.

3.4.3.2. Yoon Nelson model

The Yoon Nelson model expressed by Eq. (20) is based on the concept of the decrease in the adsorption for each adsorbate molecule is directly proportional to the probability of adsorbate breakthrough on the adsorbent.

$$\frac{C_{eff}}{C_o - C_{eff}} = \exp(K_{YN}t - \tau K_{YN}) \quad (20)$$

K_{YN} is the Yoon Nelson rate velocity constant (L/min), τ is the time in (min) required for 50% adsorbate breakthrough.

The linearized form of Yoon Nelson model is given by Eq. (21).

$$\ln\left(\frac{C_{eff}}{C_o - C_{eff}}\right) = \frac{K_{YN}}{Q}V_{eff} - \tau K_{YN} \quad (21)$$

To determine the rate constant (K_{YN}) and the time needed for 50% adsorbate breakthrough, (T) in Yoon Nelson model, experimental data were fit into Eq. (21). This equation was used to fit the experimentally obtained data by plotting $\ln\left(\frac{c_{eff}}{c_o - c_{eff}}\right)$ against the effluent volume. The Yoon Nelson rate constant and time required for 50% adsorbate breakthrough (T) were determined from the slope and intercept respectively. The values of two parameters are given in Table 7 for Ba(II) and Sr(II) at 50% breakthrough curve. The data in Table 7 also indicate that the T value of model as similar to the T_{exp} where T_{exp} is the time required for 50% adsorbate breakthrough from experiments in min. It was found that the time required for 50% adsorbate breakthrough (T) for Ba(II) and Sr(II) increased with increasing bed height but decreased with increasing flow rate due to less residence time of metal ions in adsorbent bed. Since, the experimental data goes well with the model. Therefore; Yoon Nelson model is suitable model to describe fixed bed operations.

The regeneration of loaded CACR by Ba and/or Sr was studied using 2 M HNO_3 at 25°C. To check the reusability of CACR, five successive adsorption-desorption cycles were performed. The results revealed that the adsorption capacity decreased from 100 to 98, 97, 96, 94 and 92% respectively over five cycles.

4. Conclusions

A new modified chitosan resin with pendent amidoxime moieties (CACR) was successfully prepared by reaction of cross-linked chitosan beads with acrylonitrile to support the polymer with nitrile group that facilitates the reaction of beads with hydroxylamine hydrochloride. Synthesized CACR was characterized using FTIR, TGA, DSC, SEM-EDX and surface area. This resin have high sorption capacity for Ba(II) and Sr(II) from their aqueous medium. The sorption of metal ions onto CACR is influenced by several factors such as the solution pH, concentration of metal ions, contact time and solution temperature. In batch equilibrium adsorption method, the optimum sorption pH for Ba (II) and Sr(II) were 7 and 8.5, respectively. The maximum adsorption capacity of CACR followed the order Ba(II) > Sr(II). The adsorption process follows the Freundlich isotherm model indicates that the heterogeneous sorption is dominant. The kinetic experiments showed that adsorption well fits to pseudo-second order model. Thermodynamic parameters suggest that adsorption of metal ions on CACR is spontaneous and endothermic in nature. CACR was not only efficient for Ba(II) and Sr(II) removal by batch but also by column methods, and the best condition for adsorption process at 0.5 ml/min and 1.7 cm bed height. Thomas and Yoon Nelson models are suitable models to describe fixed bed column operations. The resin was eluted using 0.2 M HNO_3 and CACR could be used repetitively for five times with more than 90% of initial sorption capacities.

References

- [1] G. Gurboga, H. Tel, Preparation of TiO_2 - SiO_2 mixed gel spheres for strontium adsorption, *J. Hazard. Mater.*, 120 (2005) 135–142.
- [2] Sh.P. Mishra, V.K. Singh, Radiotracer technique in adsorption study XIII: Adsorption of barium and strontium ions on chromium (IV) oxide powder, *Appl. Radiat. Isot.*, 46 (1995) 847–853.
- [3] M. Torab-Mostaedi, A. Ghaemi, H. Ghassabzadeh, M. Ghannadi-Maragheh, Removal of strontium and barium from aqueous solutions by adsorption onto expanded Perlite, *Can. J. Chem. Eng.*, 89 (2011) 1247–1254.
- [4] O. Celebi, A. Kilikli, H.N. Erten, Sorption of cesium and barium ions onto solid humic acid, *J. Hazard. Mater.*, 168 (2009) 695–703.
- [5] F. Gingele, A. Dahmke, Discrete barite particles and barium as tracers of pale productivity in south Atlantic sediments, *Paleoceanography*, 9 (1994) 151–168.
- [6] S. Garcia-Ruiz, M. Maladovan, G. Fortunato, S. Wunderli, J. Ignacio, Evaluation of strontium isotope abundance ratios in combination with multi elemental analysis as a possible tool to study the geographical origin of ciders, *Anal. Chim. Acta.*, 590 (2007) 55–66.
- [7] S. Chegrouche, A. Mellah, M. Barkat, Removal of strontium from aqueous solutions by adsorption onto activated carbon: kinetic and thermodynamic studies, *Desalination*, 235 (2009) 306–318.
- [8] M. Dash, F. Chiellini, R.M. Ottenbrite, E. Chiellini, Chitosana versatile semi-synthetic polymer in biomedical applications, *Prog. Polym. Sci.*, 36 (2011) 981–1014.
- [9] G.L. Dotto, M. Moura, T.R. Scadaval, L.A.A. Pinto, Application of chitosan films for the removal of food dyes from aqueous solutions by adsorption, *Chem. Eng. J.*, 214 (2013) 8–16.
- [10] M.M.H. Khalil, K.Z. Al-Wakeel, S.S. Abd El Rehim, H. Abd El Monem, Efficient removal of ferric ions from aqueous medium by amine modified chitosan resins, *J. Environ. Chem. Eng.*, 1 (2013) 566–573.
- [11] C. Xu, J. Wang, T. Yang, X. Chen, X. Liu, X. Ding, Adsorption of uranium by amidoximated chitosan-grafted polyacrylonitrile, using response surface methodology, *Carbohydr. Polym.*, 121 (2015) 79–85.
- [12] S.A.A. Farha, N.A. Badawy, A.A. El-Bayaa, S.E. Garamon, The effect of chelating agent on the separation of some metal ions from binary mixture solution by cation-exchange resin, *Nat. Sci.*, 8 (2010) 16–25.
- [13] Z. Majidnia, A. Idris, M. Majid, R. Zin, M. Ponraj, Efficiency of barium removal from radioactive waste water using the combination of maghemite, titania nanoparticles in PVA and alginate beads, *Appl. Radiat. Isot.*, 105 (2015) 105–113.
- [14] A. Ghaemi, M.T. Mostaedi, M. Ghannadi-Maragheh, Characterizations of strontium(II) and barium(II) adsorption from aqueous solutions using dolomite powder, *J. Hazard. Mater.*, 190 (2011) 916–921.
- [15] Li. Tingting, H. Fan, D.Y. Dong, Prussian blue analog caged in chitosan surface-decorated carbon nano-tubes for removal cesium and strontium, *J. Radioanal. Nucl. Chem.*, 310 (2016) 1139–1145.
- [16] A. Zhang, Y.Z. Wei, M. Kumagai, T. Koyama, Kinetics of the adsorption of strontium (II) by a novel silica-based 4,4',(5)-di(tert-butyl cyclohexano)-18-crown-6 extraction resin in nitric acid medium, *J. Radioanal. Nucl. Chem.*, 262 (2004) 739–744.
- [17] J.R. Kaczvinsky, J.S. Fritz, D.D. Walker, M.A. Ebra, The effects of reaction conditions on porous chelating polymers designed for the decontamination of nuclear waste, *J. Radioanal. Nucl. Chem.*, 116 (1987) 63–75.
- [18] M. Liu, F. Dong, W. Kang, S. Sun, H. Wei, W. Zhang, X. Nie, Y. Guo, T. Huang, Y. Liu, Biosorption of strontium from simulated nuclear wastewater by scenedesmus spinosus under culture conditions: adsorption and bioaccumulation processes and models, *Int. J. Environ. Res. Public Health*, 11 (2014) 6099–6118.
- [19] M.D. Rosario, T.D. Abreu, F.C.D.F. Barros, G.S.C. Raulino, C.P. Moura, R.F.D. Nascimento, Metal ions removal from synthetic solutions and produced water using activated zeolite, *Int. J. Eng. Res. Appl.*, 12 (2012) 20–25.

- [20] Y. Chu, R. Wang, M. Chen, Key Preliminary study on removing Cs⁺/Sr²⁺ by activated porous calcium silicate-A by-product from high-alumina fly ash recycling industry, *J. Air Waste Manag. Assoc.*, 65 (2015) 99–105.
- [21] A.M. El-Kamash, Evaluation of zeolite A for the sorptive removal of Cs⁺ and Sr²⁺ ions from aqueous solutions using batch and fixed bed column operations, *J. Hazard. Mater.*, 151 (2008) 432–445.
- [22] A.F. Shaaban, D.A. Fadel, A.A. Mahmoud, M.A. Elkomy, S.M. Elbahi, Synthesis of a new chelating resin bearing amidoxime group for adsorption of Cu(II), Ni(II) and Pb(II) by batch and fixed-bed column methods, *J. Environ. Chem. Eng.*, 2 (2014) 632–641.
- [23] A.F. Shaaban, D.A. Fadel, A.A. Mahmoud, M.A. Elkomy, S.M. Elbahi, Removal of Pb(II), Cd(II), Mn(II) and Zn(II) using iminodiacetate chelating resin by batch and fixed bed column methods, *Desal. Water Treat.*, 51 (2013) 5526–5536.
- [24] D.A. Fadel, S.M. El-Bahy, Y.A. Abdul-Aziz, Heavy metals removal using iminodiacetate chelating resin by batch and column techniques, *Desal. Water Treat.*, 57 (2016) 25718–25728.
- [25] A.F. Shaaban, D.A. Fadel, A.A. Mahmoud, M.A. Elkomy, S.M. Elbahi, Synthesis and characterization of dithiocarbamate chelating resin and its adsorption performance towards Hg(II), Cd(II) and Pb(II) by batch and fixed-bed column methods, *J. Environ. Chem. Eng.*, 1 (2013) 208–217.
- [26] D.F. Wang, B.J. Liu, Y. Xu, L. Zhang, Chinese patent: 201010119859.6.
- [27] H. Kalavathy, B. Karthik, L.R. Miranda, Removal and recovery of Ni and Zn from aqueous solution using activated carbon from Heveabrasiliensis; batch and column studies, *Colloids Surf. B.*, 78 (2010) 291–302.
- [28] C.M. Fotalan, C.C. Kan, M.L. Dalida, C. Pascua, M.W. Wan, Fixed-bed column studies on the removal of copper using chitosan immobilized on bentonite, *Carbohydr. Polym.*, 83 (2011) 697–704.
- [29] C.L. de Vasconcelos, B.M. Bezerril, D.E.S. dos Santos, T.N.C. Dantas, M.R. Pereira, J.L.C. Fonseca, Effect of molecular weight and ionic strength on the formation of polyelectrolyte complexes based on poly(methacrylic acid) and chitosan, *Biomacromolecules*, 7 (2006) 1245–1252.
- [30] R.S. Vieira, M.M. Beppu, Interaction of natural and crosslinked chitosan membranes with Hg(II) ions, *Colloids Surf. A.*, 279 (2006) 196–207.
- [31] O.A. Jr. Monteiro, C. Airoidi, Some studies of crosslinking glutaraldehyde interaction in a homogeneous system, *Int. J. Biol. Macromol.*, 26 (1999) 119–128.
- [32] Z.J. Knaull, S.M. Hudson, A.M.K. Creber, Cross linking of chitosan fibers with dialdehydes: proposal of a new reaction mechanism, *J. Polym. Sci.*, 37 (1999) 1079–1094.
- [33] N. Bilba, D. Bilba, G. Moroi, Synthesis of a polyacrylamidoxime chelating fiber and its efficiency in the retention of palladium ions, *J. Appl. Polym. Sci.*, 92 (2004) 3730–3735.
- [34] F. Eloy, R. Lenaers, The chemistry of amidoximes and related compounds, *Chem. Rev.*, 62 (1962) 155–183.
- [35] S.K. Mittal, P. Singh, Exchange kinetic studies zirconium anti mono phosphate, *Indian J. Chem., Sect A.*, 41A (2002) 500–505.
- [36] I. Langmuir, The adsorption of gases on plane surfaces of glass, mica and platinum, *J. Am. Chem. Soc.*, 40 (1918) 1361–1403.
- [37] T.W. Weber, R.K. Chakravot, Pore and solid diffusion models for fixed bed adsorbents, *AIChE J.*, 20 (1974) 228–238.
- [38] A. Sari, M. Tuzen, D. Citak, M. Soylak, Equilibrium, kinetic and thermodynamic studies of adsorption of Pb(II) from aqueous solution onto Turkish kaolinite clay, *J. Hazard. Mater.*, 149 (2007) 283–291.
- [39] X.S. Wang, J. Huang, H.Q. Hua, J. Wang, Y. Qin, Determination of kinetic and equilibrium parameters of the batch adsorption of Ni(II) from aqueous solutions by Na-mordenite, *J. Hazard. Mater.*, 142 (2007) 468–476.
- [40] H. Freundlich, Adsorption in solution, *Phys. Chem. Soc.*, 40 (1906) 1361–368.
- [41] M.J. Temkin, V. Pyzev, Recent modifications to Langmuir isotherms, *Acta Physiochim. U.S.S.R.*, 12 (1940) 217–222.
- [42] Y.S. Ho, Citation review of Lagergren kinetic rate equation on adsorption reactions, *Scientometrics*, 59(2004) 171–177.
- [43] Y.S. Ho, Review of second-order models for adsorption systems, *J. Hazard. Mater.*, 136 (2006) 681–689.
- [44] W.J. Weber, J.C. Morris, Equilibria and capacities for adsorption on carbon, *J. Sanitary Eng. Div.*, 90 (1964) 79–108.
- [45] C. Sarici-Ozdemir, Y. Onal, Equilibrium, kinetic and thermodynamic adsorptions of the environmental pollutant tannic acid onto activated carbon, *Desalination*, 251 (2010) 146–152.
- [46] A. Nilchi, R. Saberi, M. Moradi, H. Azizpour, R. Zarghami, Adsorption of cesium on copper hexacyanoferrate-PAN composite ion exchanger from aqueous solution, *Chem. Eng. J.*, 172 (2011) 572–580.
- [47] S.M. El-Bahy, Z.M. El-Bahy, Synthesis and characterization of a new iminodiacetate chelating resin for removal of toxic heavy metal ions from aqueous solution by batch and fixed bed column methods, *Korean J. Chem. Eng.*, 33 (2016) 2492–2501.
- [48] S.M. El-Bahy, Z.M. El-Bahy, Synthesis and characterization of polyamidoxime chelating resin for adsorption of Cu(II), Mn(II) and Ni(II) by batch and column study, *J. Environ. Chem. Eng.*, 4 (2016) 276–286.
- [49] M. Christine, U.F. Sala, U.P. Sala, Quantitative determination of hexavalent chromium in aqueous solutions by UV-V is spectrophotometer, *Cent. Eur. J. Chem.*, 5 (2007) 1083–1093.
- [50] N. Yahaya, I. Abustan, M. Latiff, O.S. Bello, M.A. Ahmad, Fixed-bed column study for Cu (II) removal from aqueous solutions using rice husk based activated carbon, *Inter. J. Eng. Technol.*, 11 (2011) 248–252.
- [51] A. Shahbazi, H. Younesi, A. Badiie, Batch and fixed-bed column adsorption of Cu(II) and Cd(II) from aqueous solution onto functionalized SBA-15 mesoporous silica, *Can. J. Chem. Eng.*, 91 (2013) 739–750.
- [52] S. Singha, U. Sarkar, S. Mondal, Transient behavior of a packed Column of eichhorniacrassipes stem for the removal of hexavalent chromium, *Desalination*, 297 (2012) 48–58.
- [53] O. Hamdaoui, Dynamic sorption of methylene blue by cedar sawdust and crushed brick in fixed bed columns, *J. Hazard. Mater.*, 138 (2006) 293–303.
- [54] R. Han, D. Ding, Y. Xu, W. Zou, Y. Wang, Y. Li, L. Zou, Use of rice husk for the adsorption of Congo red from aqueous solution in column mode, *Bioresour. Technol.*, 99 (2008) 2938–2946.
- [55] R. Han, Yu. Wang, X. Zhao, Y. Wang, F. Xie, J. Cheng, M. Tang, Adsorption of methylene blue by phoenix tree leaf powder in a fixed-bed column: experiments and prediction of breakthrough curves, *Desalination*, 245 (2009) 284–297.
- [56] M. Calero, F. Hernáinz, G. Blázquez, G. Tenorio, M.A. Martín-Lara, Study of Cr (III) biosorption in a fixed-bed column, *J. Hazard. Mater.*, 171 (2009) 886–893.